The Mechanism of Hydrogen Formation Induced by Low-Energy Electron Irradiation of Hexadecanethiol Self-Assembled Monolayers

Etienne Garand and Paul A. Rowntree*

Département de chimie, Université de Sherbrooke, Centre for Self-Assembled Chemical Systems, Sherbrooke, Québec, Canada J1K 2R1

Received: February 16, 2005; In Final Form: April 13, 2005

The desorption of molecular hydrogen during low-energy electron irradiation of self-assembled monolayers containing *n*-alkanethiols has been previously reported, yet to date, there is no consensus as to the mechanism for the formation of this ubiquitous product. In this study, mixed monolayers containing known ratios of perhydrogenated and perdeuterated alkanethiols were chemisorbed to Au(111)/mica substrates and used as targets for low-energy electron irradiation; by measuring the electron-stimulated production of H_2, D_2, and HD as a function of the film composition, we unambiguously show that the desorbing molecular hydrogen is formed via a two-step bimolecular reaction process. The initial electron−molecule scattering event produces a reactive atomic fragment, which then abstracts a hydrogen atom from a nearby molecular site to produce the measured bimolecular yields; the contribution of one-step unimolecular dissociation channels to the overall molecular hydrogen yields is below the ∼5% detection limit. The dependence of the electron-induced modifications to the film on the incident electron energy suggests that the primary event is dissociative electron attachment, and that the primary reactive fragment is most likely H^-. Quantitative analysis of the product yields shows that while ∼80% of the molecular hydrogen is formed by this bimolecular mechanism within the film, the remaining 20% is formed from reactive atomic fragments that are ejected from the film and subsequently react with residual H_2O adsorbed on the chamber walls.

1. Introduction

In the past decade, self-assembled monolayers (SAMs) have attracted growing attention in many areas of practical applications such as protein microsensors, electrochemical interfaces, microelectronics development, and surface passivation. Simple monolayers are easy to prepare and if sufficient attention is given to the substrate preparation and deposition conditions, the well-ordered structures can provide an excellent model system for experimental and theoretical characterizations of molecular structure and the dynamics of chemisorbed molecules. Since many of the standard surface characterization techniques (and technological applications) of thin films involve inelastic interactions with charged and energetic particles, understanding the electron-induced process within these films at the molecular level becomes increasingly important.[1] For example, electron beams used in conventional LEED (∼100 eV) can cause irreversible degradation of LB films[2] and *n*-alkanes SAMs,[3] although low-current LEED instrumentation can now preclude these effects and enable structural determinations of chemisorbed thiol systems.[4,5] Electron beams involved in HREELS (3−10 eV) have been used to study resonant excitation and dissociation in organometallic films, and film degradation during XPS analysis has been shown to be due to the reactive scattering of the photoelectrons within the organic films rather than the incident photon flux.[6−8] The specific study of low-energy electron interactions with SAMs is also motivated by lithographic considerations; it is well understood that the scattering of secondary electrons (<20 eV) limits the spatial resolution of high-energy electron beam patterning of resist materials, and recent work[9] suggests that it is the scattering of these electrons within the adsorbate layer, and not within the substrate, that imposes the ultimate resolution limits. This is therefore an important consideration for scanning probe based methods that use localized tunneling or ballistic low-energy electrons for nanolithography on SAMS.[10−13] Low-energy electron-induced structural and chemical degradation in the film has been observed with a number of techniques for *n*-alkanethiolate[12−14] and other functionalized thiolate-based SAMs.[15−19] From these works it has become clear that there is significant damage introduced into C−H, Au−S, and S−C bonding sites, principally leading to C−H bond rupture and the creation of unsaturated C−C bonds. These chemical modifications are often accompanied by the physical modifications to the macroscopic film structure and the introduction of structural defects and intermolecular cross-links, as has been observed for poly-aromatic thiol based SAMs using 50 eV electrons.[18] Desorption of molecular fragments has been used to probe the volatile products evolving from electron impact on SAMs,[19−21] confirming these chemical modifications. Cyganik et al.[19] have recently reported that irradiation of aromatic thiol SAMs with 150−1000 eV electrons can induce Au−S and S−C bond ruptures, leading to the elimination of entire thiolated film constituents. Molecular hydrogen is by far the most important volatile product of low-energy electron-induced degradation for simple *n*-alkanethiol based SAMs, especially in the <20 eV regime that is the subject of this work.

Although the detection of desorbing particles provides clear evidence for the chemical consequences of low-energy electron scattering processes within the adsorbed films, the mechanism

* Address correspondence to this author. E-mail: paul.rowntree@usherbrooke.ca.

10.1021/jp050817k CCC: $30.25
Published on Web 06/15/2005

for their formation and release from the film has not been studied in detail. In particular, our specific interest is in the application of low-energy processes to induce selective modifications to the film's structure and composition; this level of control necessitates a detailed understanding of how the energy is initially deposited into the film and the various reaction channels by which this energy is dissipated or thermalized. By reducing the excitation energy into the range of chemical processes, site-specific bond rupture can be envisioned. Following the seminal works of Sanche and co-workers,[22,23] it is now understood that resonant dissociative electron attachment (DEA) is a significant channel for the initial deposition of energy into condensed phase systems and the generation of molecular fragments, and that in many cases the surface processes can be directly compared to their gas-phase analogues. DEA can be described as a two-step process, initiated by the capture of the incident electron leading to electronic excitation to a repulsive anionic potential energy surface; this is then followed by the fragmentation into anionic and neutral species ($AB + e^- \rightarrow AB^{*-} \rightarrow A + B^-$). Much of our knowledge of the DEA process originates with simple diatomic, triatomic, or halogenated molecules in the gas phase; these works have traditionally been based upon the detection of the anionic fragments as a function of incident electron energy (E_i), and the analysis of excess energy partitioning among the fragments. It is important to note that the low density of the gas-phase environment reduces the probability of secondary reactions of the newly formed anion species. In the case of the gas-phase alkanes, the dominant anionic fragment detected is always H^-. Dorman[24] and von Trepka[25] have measured the electron energy dependence (0−16 eV) of the H^- yields in a series of saturated hydrocarbons (methane to butane) in the gas phase; for each target species the H^- yields showed a distinct maximum at $E_i = 9-10$ eV, with longer chains exhibiting the maximum yields at slightly lower energies. The onsets for H^- formation were systematically observed near $E_i = 5$ eV, well above the 3−4 eV thermodynamic threshold for the dissociation process. The presence of a distinct maximum in the anion yield curve and nonthermodynamic energetics are two of the characteristics for the resonant (i.e. state-to-state) DEA process. Rowntree et al.[26] have studied the desorption of H^- from condensed amorphous hydrocarbon films, and have reported a strong resonant process at $E_i = 10$ eV for this dominant anion fragment; although the shape and energetics of the H^- yield curves demonstrated less chain length dependence than found in the gas phase, the presence of the DEA channel was clearly demonstrated for the condensed phase *n*-alkane systems.

To our knowledge, direct detection of anion fragments from *n*-alkanethiol SAMs during low-energy electron irradiation has not yet been reported; this is partially due to the experimental requirements for load-lock facilities and ex situ sample preparation protocols. DEA processes leading to C−H bond rupture in these monolayers have been inferred based on the depletion of the C−H vibrational bands induced by low-energy electron irradiation;[14] the maximum cross section for the depletion of the CH_3 and CH_2 stretching mode absorbances is systematically found at $E_i = 9-10$ eV, thus correlating well with the DEA profiles measured by anion detection from amorphous condensed phases studies.

The dependencies of H_2 yields on the incident electron energy from 5 to 20 eV[20] correlate with the H^- yields of DEA in the gas[24] and condensed[26] phase of *n*-alkanes suggesting that hydrogen formation is mostly initiated by the preparation of electronically excited anionic resonant states. The mechanism of hydrogen formation was initially concluded to be a bimolecular process based on the observation of H_2 yields that depended quadratically upon the atomic hydrogen content, *m*, in the chemisorbed C_nH_mS- species;[20] this interpretation presumed a uniform degradation of the film (i.e. no site selectivity). The most probable reaction pathway is the abstraction of a proton or a hydrogen atom from C−H by H^- and the formation of H_2 or short-lived H_2^-. Such a post-DEA secondary reaction has been reported for a condensed O_2 film mixed with *n*-alkanes,[22,23] where desorption yield distribution of the OH^- was energetically similar to that of the H^- generated from DEA to the alkane film constituents. However, a subsequent infrared study[14] on electron-irradiated alkanethiol SAMs has clearly demonstrated that dehydrogenation is *not* uniformly distributed throughout the film but preferentially localized near the film−vacuum interface. The lifetime of the excited state is reduced by the metal substrate via dipole−image dipole quenching and thus leads to a distant-dependent bond-rupture probability as presented by Olsen and Rowntree.[14] Tai et al.[27] have reported that 10 eV electron irradiation of terphenylthiol SAMs induces distance-dependent interchain polymerization profiles, which was also ascribed to this quenching mechanism.[14] Recently, a low-energy ESD study from functionalized alkanethiol SAMs[21] also concluded that most of the molecular hydrogen detected originates at the film−vacuum interface, where the scattering probability by H^- is significantly reduced; based on this observation, an alternate one-step (unimolecular) resonant mechanism was proposed that leads to *direct* elimination of H_2 or H_2^-. Similar molecular fragmentation channels have been invoked to interpret the formation of D_2 from electron-irradiated condensed D_2O[28] or O_2 from gas-phase CO_2.[29] Bond rearrangement involved in this mechanism can be promoted by a highly excited bending (or scissor) mode during the lifetime of the transient molecular anion or shortly after electron autodetachment. Thus far, no experiments directly probing the possible channels for hydrogen formation in SAM systems have been performed and as a result the mechanism remains far from certain for these condensed phase environments.

In this paper, we report the mass-selected detection of hydrogen produced during low-energy electron irradiation in mixed SAMs containing fully hydrogenated hexadecanethiol (h_{33}-C16) and its fully deuterated analogue (d_{33}-C16); the film composition (i.e., the isotopic *h*:*d* ratio) was controlled via the initial solution used to prepare the SAM. In this text, "hydrogen" will be used to *collectively* refer to H_2, HD, and D_2; chemical formulas will be used if isotopic specificity is required. Isotopic labeling provides a clear distinction between unimolecular and bimolecular channels, and allows us to quantify the relative probability of each pathway in the case of multichannel (and multicomponent) systems. This method has been successfully used by Dyne and Jenkinson[30−32] to elucidate the mechanism of hydrogen formation in the radiolysis of hydrocarbons; the present work is the first application of this method to the study of resonant processes, and the first in self-assembled monolayers. Our analysis, based on first- and second-order mathematical models of the isotopic composition of the hydrogen evolved expressed as a function of the isotopic composition of the SAM, demonstrates that the formation of hydrogen by DEA in SAMs occurs exclusively via a bimolecular channel.

Whereas most studies on electron- and photon-irradiated SAM systems have been performed at room temperatures, the present work was conducted at 25 K. Our previous work on the electron irradiation of *n*-alkanethiol SAMs[33,34] has shown that the infrared

signatures of the electron-induced damage processes in the 0−20 eV regime are more clearly resolved under these conditions, due to the suppression of the disordering features of the film at low temperatures that severely complicate the interpretation of the spectra for irradiation at ambient temperatures. Feulner et al.[35] have recently shown that mass transport of heavy molecular fragments during 270−315 eV photolysis is significantly reduced at 50 K; the movement of atomic fragments and hydrogen abstraction reactions were relatively unaffected by the sample temperature. Our use of low-temperature samples is also motivated by the use of Xe overlayers to trap the molecular hydrogen and to improve the signal to noise of the subsequent mass-selective analysis. We show herein that the Xe layers do not interfere with the main conclusions of this paper concerning the discrimination of the unimolecular vs bimolecular nature of the hydrogen elimination reaction.

The results presented in this work are intended to discriminate between two fundamentally different processes leading to the release of molecular hydrogen during low-energy electron irradiation. The first mechanism, unimolecular in nature, proceeds by the simultaneous rupture of two C−H bonds and the concerted formation of a H−H bond.

$$R{-}CH_x + e^- \rightarrow R{-}CH_{x-2} + H_2^{(-)} \qquad (1a)$$

The second, bimolecular, process involves two independent steps, which may be temporally separated by several picoseconds and distance separated by several nanometers.

$$R{-}CH_x + e^- \rightarrow R{-}CH_{x-1} + H^{(-)} \qquad (2a)$$

$$H^{(-)} + R'{-}CH_x \rightarrow R'{-}CH_{x-1} + H_2 \qquad (2b)$$

The ultimate fate of the incident electron cannot be deduced on the basis of neutral particle detection, and will not be explicitly considered in this work. The mathematical model used to analyze these mechanisms is presented below, followed by the application to the experimental results.

2. Experimental Section

Au films (150 nm thick) were evaporated onto freshly cleaved mica sheets (ASTM-V2 Techniglass) in an all-metal turbo-molecular-pumped system based on the modified protocol of DeRose et al.;[36] this has been shown to prepare high-quality films with a strongly Au(111) texture. Mica sheets were degassed at 300 °C for 12−20 h prior to deposition and annealed at the same temperature for 2 h following Au deposition. Gold substrates that were not used immediately after preparation were stored under argon atmosphere until use. Gold films were cleaned with sulfochromic acid to eliminate adventitiously adsorbed hydrocarbon material, rinsed with copious quantities of deionized water, and then cut to size and immersed in 1 mM thiol/methanol solution for at least 24 h. This protocol for the preparation of gold substrates and SAMs has been used for a number of studies in our laboratory and has been shown to form highly ordered films. Previous characterizations have included STM[37,38] and IRRAS[14,39] measurements. Hexadecanethiol (h_{33}-C16) was used as received (Aldrich, 95%) and fully deuterated hexadecanethiol (d_{33}-C16) was synthesized from d_{31}-palmitic acid (Cambridge Isotope Laboratories, 98%) following a modification of Badia's protocol[40] as described in detail previously.[39] Briefly, d_{31}-palmitic acid was reduced with $LiAlD_4$ (Aldrich 98%) to the corresponding alcohol and was then treated under reflux with 48% HBr giving the d_{33}-bromohexanedecane. Finally, the d_{33}-bromohexadecane was treated with $Na_2S_2O_3$ under reflux and the resulting Bunte salt was hydrolyzed with HCl to give the desired d_{33}-hexadecanthiol. Final purification of the thiol was by flash chromatography. Purity of the synthesized d_{33}-C16 was shown to be >99% by GC/MS. For the mixed (*h*,*d*) monolayers, the deposition solutions were prepared from appropriate volumes of the pure 1.0 mM h_{33}-C16 and d_{33}-C16 solutions. A previous IRRAS study with similar h_{33}-C16 and d_{33}-C16 mixed monolayers[39] has shown that the hydrogenated and deuterated molecules are homogeneously and randomly distributed in the film with no preferential adsorption from solution. This is consistent with thermodynamic considerations[41] that show that isotopic segregation is not expected for chains containing fewer than 30−40 carbon atoms deposited at room temperature. It should be noted that *if* segregation did occur, it would bias the results in favor of the unimolecular reaction model; as will be shown below, the observation that the unimolecular channel has a negligible contribution to the total hydrogen yields supports the hypothesis that segregation can be neglected.

The use of ex situ film preparation protocols and the large number of samples in this study required the use of a load-lock sample introduction facility for the UHV instrumentation. Samples were secured to copper carrier plates by using two copper straps to provide thermal and electrical contact to the front-surface gold film. These plates are supported on a 5-axis manipulator (Thermionics) by two rear-facing protrusions and a tab extension in the plane of the sample that fits loosely into a Ga-filled "well" on the manipulation stage, providing a rigid link when cooled below the freezing point of Ga. Samples were transferred via a turbo-pumped load-lock into our in-house designed IRRAS vacuum system (240 L/s TNB-X ion-pumped, base pressure 5×10^{-11} Torr) and mounted onto the sample stage with use of a UHV-wobble-stick. A 25 W heater is mounted into the sample support block, and OFHC copper braids connect the sample support to the tip of a closed cycle He cryostat head (APD Cryogenics Model 21-B) while permitting unrestricted sample movement. The sample support was electrically and thermally isolated from the manipulator by using glass beads as the tilt pivot points; electrical insulation from the (grounded) cryostat was via a sapphire plate sandwiched between OFHC plates attached to the OFHC copper braids. Temperatures were measured with a 0.07% Fe/Au thermocouple attached to the sample support, and a commercial controller system (Omega Engineering CYC-3000) maintained temperature control within 1 K; all irradiations were performed at the 25 K base temperature of the sample holder. The IRRAS components are arranged on a single flange containing twin differentially pumped NaCl windows. Two adjustable internal mirrors served to reflect the incident infrared beam from a conventional FTIR bench (Magna 560) onto the surface at grazing incidence (85° from the surface normal) and to direct the divergent reflected beam onto an external InSb detector. Custom LabVIEW-based software was used to control the spectrometer operation, acquire data, and present the spectra for analysis and interpretation. Typical spectrometer parameters were 2 cm^{-1} resolution (1 cm^{-1} data point spacing), 2 cm/s moving mirror velocity, with Happ−Ganzel apodization, with no zero-filling; 128−256 mirror scans were co-added to produce each measured reflectivity vs wavenumber profile. Spectra are reported herein as absorbance spectra, whereby the reference is the reflectivity of a pristine Au/mica surface.

The axis of a custom-built low-energy electron source is aligned perpendicularly to the IRRAS flange, between the two NaCl windows. This source uses three cylindrical lenses to deliver the electron beam (1−10 μA) from a resistively heated Ta disk filament (Kimball Physics) to the surface at normal incidence. Two orthogonal fields between the final lens and the surface are used to center the beam onto the surface and to raster it (10−100 Hz) across the sample to ensure uniform irradiation. The energy of the electron flux is established by the potential between the center of the filament and the surface with an estimated accuracy of ±0.5 eV and the breath of the energy distribution is estimated to be 0.3−0.4 eV (full-width at half-maximum). The sample is maintained at −2 V with respect to the chamber ground to prevent very low-energy electrons that have scattered off the lenses or deflectors from reaching the surface. Beam currents were measured on the biased substrate and were recorded to quantify the absorbed charge.

The vacuum chamber is equipped with a 1−200 amu residual gas analyzer (Stanford Research Systems, RGA-200) that simultaneously monitored the desorption yields of the pertinent neutral species. The relative sensitivity of the RGA toward HD and D_2 was calibrated by using the product of the reaction between $LiAlD_4$ (Aldrich, 98%) and deionized H_2O or D_2O (Aldrich, 99.96%). A homemade stainless steel reactor was attached directly to the gas ramp of the vacuum chamber. The sealed reactor containing separate $LiAlD_4$ and frozen H_2O (D_2O) was pumped down and then an on/off valve allowed $LiAlD_4$ to "fall" on the thawing water. The resulting HD (D_2) was immediately transferred and stored in the gas manifold via a liquid-nitrogen cooled trap to remove all traces of water. Purity of the separate HD and D_2 products was verified with the RGA; a 1:1 mixture was then prepared with a Baratron absolute pressure transducer (MKS) and introduced in the chamber. The relative sensitivity of the RGA was given by the ratio of two peak heights for equivalent partial pressure of HD and D_2. This experimental ratio ($S_{D_2}/S_{HD} = 0.72 \pm 0.05$) is in reasonable agreement with the ratio of $(M_{D_2}/M_{HD})^{-1/2} = 0.87$ proposed by the manufacturer, based on the theory of the ideal quadrupole filter.[42]

To increase the signal/noise ratio, especially with the very diluted SAMs, the hydrogen produced during the irradiation process was concentrated by trapping in a Xe multilayer that was deposited onto the methyl-terminated SAM surface prior to electron irradiation. Heating the irradiated Xe/SAM systems caused a rapid desorption of the embedded products and yielded strong and reproducible RGA signals for HD and D_2 even when the deuterated fraction in the film was below 25%. For the results reported herein, substrates were cooled to 25 K and 80 L of xenon (Praxair, 5.0 research grade) were dosed onto the surface from a background pressure of 1×10^{-7} corrected for the gauge sensitivity (Varian). The Xe/SAM systems were irradiated at the preselected energy, ranging from 9 to 11 eV, until the total absorbed charge was 2 mC/cm^2. No hydrogen was detected by RGA during the irradiation process confirming the quantitative trapping of the volatile products. The substrates were then heated from 25 to 100 K at a rate of 10 K/min and the desorption profiles of m/z 3, 4, and 132 were simultaneously measured. H_2 was also monitored but due to (1) the residual background gas and (2) the possible trapping of this hydrogen on the xenon layer (thus creating a fictitious desorption profile of H_2), this information was not used in the data analysis reported herein; this work will concentrate on the behavior of HD and D_2 yields as the isotopic composition of the film is varied.

It should be noted that although dissociation of the trapped H_2 via the anionic $^2\Sigma_g^+$ state or the neutral $^3\Sigma_u^+$ state is possible with 10 eV electrons, the cross sections for these processes are much smaller than those of the primary dissociation processes in the alkanethiol monolayers, which are ~5 Å^2 for C_{16} SAMs.[14] Rapp et al.[43] have found that the cross section for the anionic dissociation channel is $\sim 1.3 \times 10^{-4}$ Å^2 at 10 eV in the gas phase; Khakoo and Segura[44] have found that the cross section for the neutral dissociation channel in the gas phase is only 0.2 Å^2, and it is expected that this would be further reduced in the Xe matrix due to caging and recombination processes. Thus, the quantity of reactive fragments that could be produced by this type of secondary process is significantly lower than the yield by the primary dehydrogenation mechanism(s) in the SAM. Combined with the less-than-unity reaction probabilities of these fragments with the SAM, we conclude that the isotopic "scrambling" of the experimental HD and D_2 yields by these fragments is a very small effect; the negligible impact on the conclusions of this study is confirmed by our experimental results, as described below.

3. Result and Discussion

3.1. Mathematical Model. To extract the mechanism of hydrogen formation from our measurements, we present a simple model involving three possible reaction channels for the production of HD and D_2 species by electron scattering in mixed (H, D) films. This model considers that a single electron initiates the process and thus reactive association of two independently produced species does not contribute to the formation of hydrogen. This approach is justified by the low electron fluxes used in these measurements; the maximum current used (5×10^{-6}A/cm^2) implies that on average, the delay between the arrival times of individual electrons to the 2 cm^2 surface is of the order of 1−10 fs, thus precluding near-simultaneous events at sufficiently small distances. Without explicitly considering the fate of the incident electron and the site of the reaction in the film, three possible processes can be proposed to generate the HD and D_2 species considered herein.

Reaction 1: Unimolecular Hydrogen Production.

$$CD_x + e^- \rightarrow CD_{x-2} + D_2 \quad (1a)$$

$$CH_x + e^- \rightarrow CH_{x-2} + H_2 \quad (1b)$$

Reaction 2: Bimolecular Hydrogen Production via Reactive Scattering in the Film.

$$CD_x + e^- \rightarrow CD_{x-1} + D \quad (2a)$$
$$D + CD_x \rightarrow CD_{x-1} + D_2$$

$$CH_x + e^- \rightarrow CH_{x-1} + H \quad (2b)$$
$$H + CD_x \rightarrow CD_{x-1} + HD$$

$$CD_x + e^- \rightarrow CD_{x-1} + D \quad (2c)$$
$$D + CH_x \rightarrow CH_{x-1} + HD$$

$$CH_x + e^- \rightarrow CH_{x-1} + H \quad (2d)$$
$$H + CH_x \rightarrow CH_{x-1} + H_2$$

Reaction 3: Bimolecular Hydrogen Production via Reactive Scattering Outside the Film.

$$CD_x + e^- \rightarrow CD_{x-1} + D \quad (3a)$$

$$D + H_2O \rightarrow OH + HD$$

$$CH_x + e^- \rightarrow CH_{x-1} + H \quad (3b)$$

$$H + H_2O \rightarrow OH + H_2$$

Reaction 1 represents the unimolecular mechanism proposed by Huels et al.,[21] which is endothermic by 4.2−5.7 eV.[45] It includes all the possible unimolecular channels for the formation of molecular hydrogen such as the concerted elimination of hydrogen from two adjacent methylene sites to form molecular hydrogen and a C═C bond. The scattering species in reaction 2 is presumed to be anionic hydrogen (H^-, D^-) based on previous DEA studies in *n*-alkanes[24,26] but the exact mechanism of the secondary reaction is not a critical consideration at this point. Abstraction of a proton will lead to desorbing hydrogen and an adsorbed carbanion, while abstraction of atomic H will result in a short-lived H_2^- and a radical in the alkane chain. Reactive scattering occurring on a single molecule is neglected in reaction 2 since the ejected $H^{(-)}$ initially follows a trajectory directed along the C−H bond axis and therefore the probability for a reaction with the parent molecule is small; the validity of this will be justified below. The scattering process in reaction 2 is endothermic by ∼0.6−1.5 eV[45] and the overall reaction is endothermic by 4.1−5.0 eV.[45] Therefore, the scattering is expected to be possible only for translationally "hot" fragments; once thermalized in the SAM or in the Xe layer, these fragments would be relatively unreactive, and could not contribute significantly to reaction 2's yield at 25−60 K. Reaction 3 considers the possibility that hydrogen is formed by the reaction of the anion with water *outside* of the film; the abundance of this species is assumed to be large with respect to the quantity of reactive incident species. Reactions between H^- and H_2O to form H_2 and OH^- have very large cross sections[46] and the anion can have enough kinetic energy[26] to escape the film and react with water adsorbed on the stainless steel walls of the chamber; H^- that is trapped in the Xe overlayer can be released upon heating, leading to a similar reaction channel with wall-adsorbed H_2O. This channel has not been taken in consideration in previous ESD studies that monitored neutral fragments, even if the mass spectrometer was not placed directly in front of the sample[20,21] or if the chamber was explicitly cooled to trap water on the walls.[20] We note that the yield of reactive fragments liberated from the SAM (i.e. reaction 3) could be reduced by the presence of the Xe layer, since such fragments could elastically scatter at the Xe:SAM interface and "rebound" toward the organic film; the Xe layer may thus increase the apparent contribution of reaction 2 with respect to reaction 3, but it cannot change the relative contributions of the unimolecular channel (reaction 1) with respect to the bimolecular channels (reaction 2 + reaction 3), and therefore the presence of the Xe layer does not affect the discrimination between the unimolecular and bimolecular channels for the formation of molecular hydrogen.

Assuming no significant isotopic effect on the relative reactivity of H/D in reaction 2, or at the dissociation step, the yield of HD and D_2 produced (Y_{HD} and Y_{D_2}, respectively) can be related to the isotopic composition in the film, expressed as mole fractions (X_D, X_H) and a constant (k_x) representing the relative contribution of each reaction pathway.

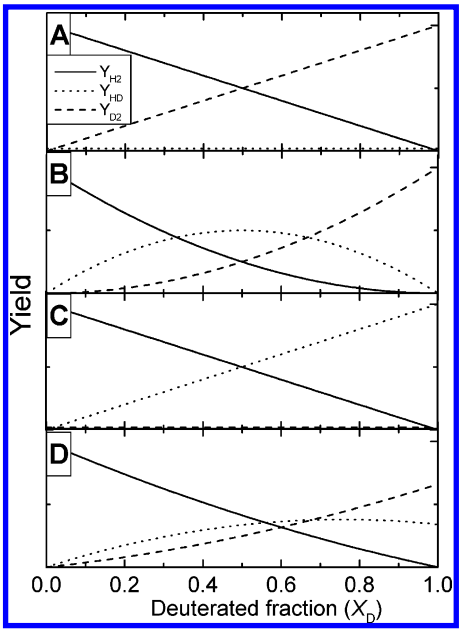

Figure 1. Calculated H_2, HD, and D_2 yields for three limiting cases for the reaction channels described in the text. Panel A shows the yields arising from a purely unimolecular dissociation mechanism, panel B shows the yields for a purely bimolecular reaction process occurring within the organic film, while panel C shows the yields for a purely bimolecular process involving the reaction of primary film-based fragments with species outside the film. Panel D shows an equally weighted combination of the above three limiting cases.

Reaction 1:

$$Y_{D_2} = k_1 X_D$$

$$Y_{HD} = 0$$

$$Y_{H_2} = k_1(1 - X_D)$$

Reaction 2:

$$Y_{D_2} = k_2 X_D^2$$

$$Y_{HD} = 2k_2 X_D X_H = 2k_2 X_D(1 - X_D)$$

$$Y_{H_2} = k_2(1 - X_D)^2$$

Reaction 3:

$$Y_{D_2} = 0$$

$$Y_{HD} = k_3 X_D$$

$$Y_{H_2} = k_3(1 - X_D)$$

Thus, the total yield of HD and D_2 produced by electron scattering can be expressed as a function of the deuterated fraction (X_D):

$$Y_{HD} = (2k_2 + k_3)X_D - 2k_2 X_D^2$$

$$Y_{D_2} = k_1 X_D + k_2 X_D^2$$

With this simple model, the relative contribution of each reaction to the total production of HD and D_2 can be easily extracted from the second-order fitting parameter of the HD/D_2 vs X_D curves. Figure 1 shows the expected trends for three limiting cases. Figure 1A represents a system where the production of hydrogen occurs only by the unimolecular channel

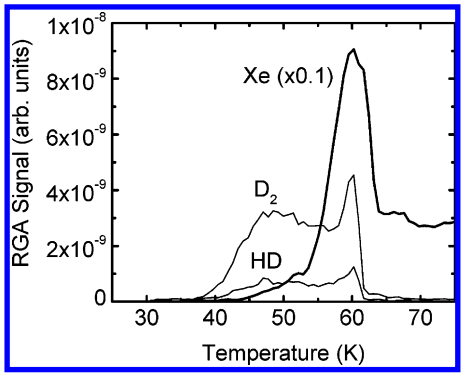

Figure 2. Typical TPD (10 K/min) profiles for HD, D_2, and Xe after the irradiation at 10 eV with a cumulative dose of 2 mC/cm^2 of a d_{33}-C16 SAM covered with 80 L of xenon.

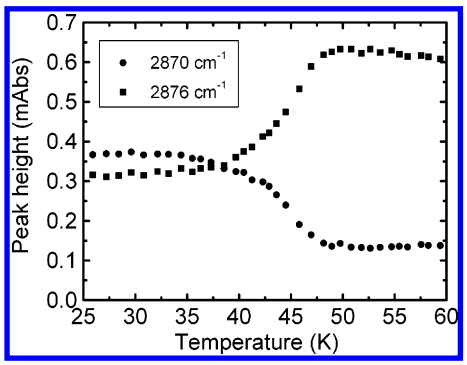

Figure 3. Intensity of the symmetric methyl stretching bands at 2870 and 2876 cm^{-1} vs temperature during the TPD (0.3 K/min) of 20 L of xenon deposited on a h_{33}-C16 monolayer.

(k_1= 1; k_2, k_3 = 0). In this case, no HD will be produced and the yield of D_2 will be linearly proportional to the fraction of deuterated molecules in the film. In Figure 1B, hydrogen is formed only by bimolecular processes in the SAM (k_2 =1; k_1, k_3=0). The yield of D_2 is proportional to X_D^2 and the HD yield curve is an inverted parabola. In Figure 1C, the bimolecular process occurring in part outside of the film produces hydrogen (k_3=1; k_1, k_2=0). The yields of H_2 and HD are linearly proportional to X_D and no D_2 is produced. Figure 1D shows an example where all three channels occur with the same probability (k_1, k_2, k_3 = $^1/_3$), such that the D_2 yield has linear and quadratic contributions from the unimolecular and bimolecular channels, respectively. The D_2 vs X_D curve will give the value of k_1 and k_2 and the HD yield in fully deuterated films will lead to k_3. Fitting of the HD vs X_D curve will provide an independent determination of k_2 and this can be used to test the physical basis of the mathematical model.

3.2. Irradiation and TPD Profile. Figure 2 shows typical TPD profiles of Xe, HD, and D_2 after irradiation (2 mC/cm^{-2}) of a d_{33}-C16 film at 10 eV. The heating rate of 10 K/min prevents significant heat transfer to the manipulator and cold copper braids, thus the peak in the xenon curve at 55−60 K is due to desorption from the sample. Vibrational spectroscopy does not allow direct detection of rare gases on the surface but the perturbation of the CH_3 termination by physisorbed species can be monitored. The presence of overlayers affects all CH_3 stretching bands but the symmetric mode at 2876 cm^{-1} exhibits the most striking perturbation. During the deposition of overlayers, the symmetric CH_3 band intensity decreases and a new peak develops at 2870 cm^{-1}; similar changes are observed for atomic (Xe) and molecular (H_2O, $Fe(CO)_5$, CO_2, C_6H_6) adsorbates.[47−49] Figure 3 presents the intensity at 2876 and 2870 cm^{-1} during the heating of a h_{33}-C16 film overlayered with xenon. The Xe desorption temperature measured in the IRRAS experiment (45−50 K) is slightly different than that with TPD but this is due to the lower heating rate of 0.3 K/min used to facilitate the acquisition of high-quality spectra.

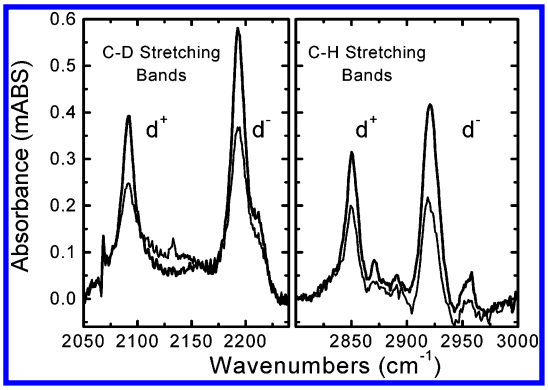

Figure 4. C−D and C−H stretching band regions of an 80% d_{33}-C16 and 20% h_{33}-C16 monolayer before (top curve in each panel) and after (lower curves) irradiation at 10 eV with a cumulative dose of 2 mC/cm^2.

The origin of the HD and D_2 products in Figure 2 is unambiguous as they are completely absent in the residual background pressure of the chamber or as contaminants in the adsorbed Xe layers. This has been verified by desorbing identical Xe films from a nonirradiated film and from films irradiated at energies below the ∼5 eV threshold discussed above; no trace of species having a m/z ratio of 3 and 4 has been detected while heating in the absence of electron irradiation. TPD curves for HD and D_2 exhibit two features. The broad HD and D_2 peaks appearing at 50 K arise from the increased diffusion of HD/D_2 within the xenon layer near the bulk desorption temperature. The second peak is sharper and strongly correlated with the Xe peak at 60 K; it is attributed to the residual HD and D_2 desorbing with the Xe overlayer. This pattern has been found to be very reproducible in all of the TPD measurements performed on post-irradiated SAMs/Xe with different isotopic compositions. Integration of the TPD profiles between 35 and 70 K provided the total amount of HD and D_2 produced during irradiation. Infrared spectroscopy also has been used to probe the induced damage in the film but also to ensure the absence of any isotopic effect such as preferential H or D depletion. Figure 4 shows the C−D and C−H regions of the spectra acquired before and after the irradiation of a sample containing 80% of deuterated molecules. This specific concentration was chosen because the similar intensity of the C−D and C−H bands allows a quantitative comparison of the signal loss induced by dehydrogenation of both hydrogenated and deuterated molecule. The C−D and C−H bands depletion ratio is 45% for both and thus indicates that no significant isotopic effects occur at the dissociative step or in subsequent scattering reactions. Any isotopic perturbation of one step would require an exactly opposite effect in the other step in order to maintain a net equivalence, which is highly improbable. The absence of an isotopic effect at the dissociation step for the long C16 chains is in agreement with the semiempirical model developed by Olsen and Rowntree[14] and with the subsequent measurements of Zharnikov et al.[12] on perdeuterated eicosanethiolate film.

3.3. HD/D_2 Yields vs Isotopic Dilution. Figure 5 presents the yields of HD and D_2 produced by irradiation (2 mC/cm^2 at 10 eV) of C16 films expressed as a function of the mole fraction (X_D) of d_{33}-C16 in the film obtained by integrating the RGA signal. Data had been corrected for the sensitivity of the RGA toward HD and D_2 and normalized so that the total hydrogen yield of the fully deuterated SAMs is 1. The nonlinear trends of the Y_{HD} and Y_{D_2} vs X_D results are similar to cases B and D

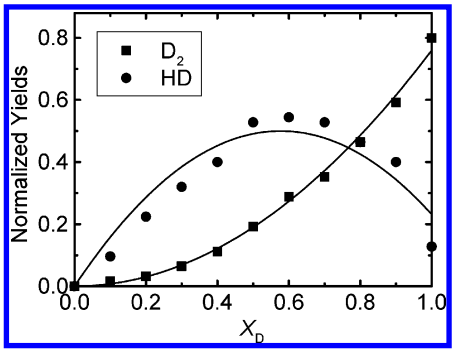

Figure 5. Yields of HD and D_2 vs the mole fraction of deuterated molecules in the film. Integration of the RGA signal is corrected for the relative isotopic sensitivity and normalized so that the total yield of hydrogen produced during the irradiation of fully deuterated SAMs at 10 eV is 1. Solid lines are the results of second-order fits of the data to the model presented in the text, and are used to extract the relative contribution (k_x) of each hydrogen formation channel.

described above, and clearly show the importance of the bimolecular hydrogen creation channel. The best fit of the D_2 yield curve is strictly proportional to X_D^2 ($k_1 = 0$) and thus allows us to conclude that the unimolecular channel (reaction 1) including any hydrogen formation pathways from a single molecule is *completely negligible.* In other words, the primary dehydrogenation process induced by low-energy electron scattering in alkanethiol SAMs does not involve the production of molecular hydrogen but a reactive fragment, presumably $H^{(-)}$, which subsequently abstracts a proton or a hydrogen atom. The absence of a significant unimolecular decomposition channel supports our neglect of (1) isotopic segregation in the film and (2) binary reactive events occurring within a single C16 molecule, since both of these processes would increase the apparent unimolecular contributions in the present study. In the present case, the D_2 yield observed can only be due to the abstraction of D from C−D bonds by deuterated projectiles and it clearly demonstrates that *much of the hydrogen formation occurs inside the film* (reaction 2a). This observation is fully supported by the inverted-parabolic shape of the HD vs X_D plot coming from the bimolecular channel involving one h_{33}-C16 and one d_{33}-C16 molecule (reactions 2b and 2c). The exact mechanism of the abstraction remains uncertain. Hydride ion could produce H_2 or H_2^- via proton or hydrogen atom abstraction, respectively. Abstraction of a proton would initially produce a negative charge on the alkane chain, perhaps leading to a gradual accumulation of charge in the film; no surface charging was detected in this study, indicating that film neutralization time scales are short. Although the reactive mean free path of the scattering species inside the SAM is unknown, it can significantly contribute to the resolution limitation of electron-beam lithographic patterning. Also, this reaction implies that the dehydrogenation cross sections extracted from the loss of C−H optical absorption[14] during electron irradiation are larger than the primary dissociation cross sections since the interaction of one electron at one molecular site may ultimately lead to the dissociation of up to two C−H bonds.

Another important feature in Figure 5 is the production of significant quantities of HD during electron irradiation of perdeuterated SAMs; these results show that for 100% deuterated SAMs, approximately 20−25% of the total hydrogen detected is in the form of HD. Examination of the IRRAS spectra of these films prior to electron irradiation shows no evidence of C−H vibrational bands; previous work has shown that the intrinsic absorption intensities of the C−H stretching modes are approximately 5× more intense than their C−D stretching counterparts, which should make their spectral signatures evident even at low concentrations. GC/MS shows no evidence of hydrogenated alkanethiol contaminants, leading us to estimate that the hydrogenated impurity content in these perdeuterated SAMs is below 2%. This minor amount of hydrogenated impurity within the SAM cannot be the origin of the HD yields. Therefore, this HD must be formed by a scattering reaction of the $D^{(-)}$ primary products with hydrogenated species outside of the film (reaction 3). The origin and the nature of the hydrogen-containing molecule outside of the film are uncertain but the most probable species is water. H^- is known to easily react with water to produce $H_2 + OH^-$,[46] and H_2O is a ubiquitous contaminant in the chamber volume and more importantly under the UHV conditions of these experiments, on the stainless steel walls of vacuum chamber. Reaction of D^- with water on the chamber walls would require that trapped anions would have enough energy to overwhelm the ∼1 eV polarization barrier required for desorption. Whatever the mechanism for the formation of this HD, the key conclusion is that approximately 20−25% of the primary dissociation products can escape and react outside the film. This result is in agreement with a previous study[26] where significant desorption yield of H^- evolving from DEA in condensed amorphous hydrocarbon films was detected. This mechanism could also contribute to the detected H_2 in systems where the quadrupole was not measuring line-of-sight desorption directly from the film[20,21] and where the chamber walls were explicitly cooled to trap water.[20]

As discussed above, it is conceivable that electron-induced dissociation of the trapped molecular hydrogen may lead to reactive H, D, H^-, and/or D^- fragments, which could then react with the substrate SAM. If the yield of this process was significant, the measured HD and D_2 yields would reflect the convolution of the initial formation mechanisms with the "scrambling" effect of these generated fragments reacting against the SAM; further consideration is warranted to ensure that such processes cannot lead to confusion as to the primary dehydrogenation mechanism. We can imagine a "worst-case scenario", whereby the primary dehydrogenation process in the SAM leads to $H_2 + D_2$ via unimolecular dissociation channels, and that the measured HD is the result of an electron-induced dissociation of this molecular hydrogen (via the $^3\Sigma_u^+$ state) and subsequent efficient reaction of the atomic H with deuterated SAM components or D with the hydrogenated SAM components. The HD:D_2 yield ratio would be directly proportional to electron-induced dissociation probabilities of the molecular hydrogen; less efficient reactions between fragments and the SAM would reduce this "scrambled channels" contribution and make the primary dissociation mechanism(s) more evident. The low cross sections for the electron-induced dissociation of hydrogen at 10 eV[44] suggest that this contribution would be small, but we note that these cross sections increase by a factor of 4 as the incident electron energy is increased from 9.2 to 12.2 eV,[44] with a pronounced maximum at 15.2 eV. We have repeated our studies using incident electron energies of 9 and 11 eV and 50:50 h_{33}:d_{33} SAM films; although the *absolute* yields of the various species are influenced by the incident energy, the *relative* HD:D_2 yields are constant within the 5% experimental precision. The absolute intensities have a maximum at 10 eV, as expected for the resonant processes characteristic of the dissociative electron-alkane scattering,[14,24,25] but show no evidence of a skewed distribution toward enhanced HD formation at higher energies as would be the case for molecular dissociation via the $^3\Sigma_u^+$ state. Thus, the large magnitude *and*

TABLE 1: Contributions of Individual Processes to Total Hydrogen Yields

	process	k_x
reaction 1	unimolecular	$k_1 < 0.05$
reaction 2	bimolecular, inside the film	$k_2 = 0.77 \pm 0.01$
reaction 3	bimolecular, outside the film	$k_3 = 0.23 \pm 0.09$

the energetic profiles of the HD:D_2 yields confirm that electron-induced dissociation of H_2 and D_2 is negligible under the conditions of our work, and that the primary hydrogen elimination process is bimolecular in nature.

Table 1 presents the normalized occurrence (k_x) extracted from the second-order fitting parameter of the HD/D_2 vs X_D curves for each hydrogen formation channel. The values of k_1 (negligible) and k_2 (0.77 ± 0.01) are from the quadratic fit of D_2 vs X_D; k_3 (0.23 ± 0.09) is determined with the yield of HD at $X_D = 1$. It should be noted that k_2 can also be independently determined from the fit of the HD vs X_D curve; the resulting value of 0.76 ± 0.08 is in excellent agreement with the k_2 derived from the D_2 yield.

4. Conclusion

The results presented in this work demonstrate that isotopic labeling can be used to probe the mechanism of reactive processes in self-assembled organic films. The key conclusion of this study is that the molecular hydrogen detected during low-energy electron irradiation near 10 eV in hexadecanethiol SAMs is created exclusively via a bimolecular channel. The primary electron-induced processes lead to the formation of atomic or anionic hydrogen fragments; the yield of reactions that proceed by direct dissociation into molecular hydrogen is below our ability to measure. This study shows that the secondary reactions are dominated by the interaction of the primary fragments with nearby alkanethiol adsorbates leading to the creation of molecular hydrogen. The detection of the neutral products of these reactive encounters does not directly identify the nature of the reactive species that is created by the electron irradiation (i.e., to discriminate between H and H^-), but the close similarity of the energy dependence of the hydrogen yield obtained during irradiation of SAMs to that of the H^- yield from amorphous alkane solids strongly suggests that the initial event is dissociative electron attachment. The majority of these primary $H^{(-)}$ fragments react with the film itself, with approximately 20−25% escaping the film to react with system impurities; in the experiments reported herein, these reactions would occur during the thermal cycling of the Xe layer, while experiments that directly measure ESD yields would provoke these processes in real time.

Finally, we note that the secondary scattering reactions within the film can significantly increase the observed cross section for the low-energy induced degradation of alkanethiol SAMs, since approximately 1.75 C−H bonds are broken per primary electron−molecule dissociation event. Characterization of this secondary reaction requires more study and would provide useful information for lithographic applications. The effective range of the primary dissociation fragments within the film (prior to thermalization or reaction) may present a fundamental limit for high-resolution lithographic techniques, and would merit further study.

Acknowledgment. Financial support from NSERC (Canada) and FQRNT (Québec) is gratefully acknowledged. The authors thank Prof. A. Badia (Université de Montréal) for providing details of her synthetic methods for the preparation of the perdeuterated thiols.

References and Notes

(1) Duwez, A.-S. *J. Electron Spectrosc. Relat. Phenom.* **2004**, *134*, 97.
(2) Vogel, V.; Woll, C. *J. Chem. Phys.* **1986**, *84*, 5200.
(3) Dubois, L. H.; Zegarski, B. R.; Nuzzo, R. G. *J. Chem. Phys.* **1993**, *98*, 678.
(4) Loepp, G.; Vollmer, S.; Witte, G.; Wöll, Ch. *Langmuir* **1999**, *15*, 3767.
(5) Azzam, P.; Cyganik, P.; Witte, G.; Buck, M.; Wöll, Ch. *Langmuir* **2003**, *19*, 8262.
(6) Graham, R. L.; Bain, C. D.; Biebuyck, H. A.; Laibinis, P. E.; Whitesides, G. M. *J. Phys. Chem.* **1993**, *97*, 9456.
(7) Laibinis, P. E.; Graham, R. L.; Biebuyck, H. A.; Whitesides, G. M. *Science* **1991**, *254*, 981.
(8) Xia, Y.; Whitesides, G. M. *Angew. Chem., Int. Ed.* **1998**, *37*, 550.
(9) Silvis-Cividjian, N.; Hagen, C. W.; Leunissen, L. H. A.; Kruit, P. *Microelectron. Eng.* **2002**, *61*−*62*, 693.
(10) Lercel, M. J.; Redinbo, G. F.; Craighead, H. G.; Sheen C. W.; Allara, D. L. *Appl. Phys. Lett.* **1994**, *65*, 974.
(11) Lercel, M. J.; Rooks, M.; Tiberio, R. C.; Craighead, H. G.; Sheen, C. W.; Parikh, A. N.; Allara, D. L. *J. Vac. Sci. Technol. B* **1995**, *13*, 1139.
(12) Zharnikov, M.; Frey, S.; Heister K.; Grunze, M. *Langmuir* **2000**, *16*, 2697.
(13) Zharnikov, M.; Geyer, W.; Golzhauser, A.; Frey S.; Grunze M. *Phys. Chem. Chem. Phys.* **1999**, *1*, 3163.
(14) Olsen, C.; Rowntree, P. *J. Chem. Phys*. **1998**, *108*, 3750.
(15) Frey, S.; Rong, H.-T.; Heister, K.; Yang, Y.-J.; Buck M.; Zharnikov, M. *Langmuir* **2002**, *18*, 3142.
(16) Frey, S.; Heister, K.; Zharnikov M.; Grunze, M. *Phys. Chem. Chem. Phys.* **2000**, *2*, 1979.
(17) Heister, K.; Frey, S.; Golzhauser, A.; Ulman A.; Zharnikov, M. *J. Phys. Chem. B* **1999**, *103*, 11098.
(18) Geyer, W.; Stadler, V.; Eck, W.; Zharnikov, M.; Gölzhäuser, A.; Grunze, M. *Appl. Phys. Lett.* **1999**, *75*, 2401.
(19) Cyganik, P.; Vandeweert, E.; Postawa, Z.; Bastiaasen, J.; Vervaecke, F.; Lievens, P.; Siverans, R. E.; Winograd, N. *J. Phys. Chem. B* **2005**, *109*, 5085.
(20) Rowntree, P.; Dugal, P.-C.; Hunting D.; Sanche, L. *J. Phys. Chem.* **1996,** *100*, 4546.
(21) Huels, M. A.; Dugal P.-C.; Sanche, L. *J. Chem. Phys.* **2003**, *118*, 11168.
(22) Sanche, L.; Parenteau, L. *J. Chem. Phys*. **1990**, *93*, 7476.
(23) Sanche, L.; Parenteau, L. *Phys. Rev. Lett.* **1987**, *59*, 136.
(24) Dorman, F. H. *J. Chem. Phys.* **1966**, *44*, 3856.
(25) von Terpka, L.; Neuert, H. *Z. Naturforsh., A* **1963**, *18*, 1295.
(26) Rowntree, P.; Parenteau, L.; Sanche, L. *J. Phys. Chem.* **1991**, *95*, 4902.
(27) Tai, Y.; Shaporenko, A.; Eck, W.; Grunze, M.; Zharnikov, M. *Langmuir* **2004**, *20*, 7166
(28) Kimmel, G. A.; Orlando, T. M. *Phys. Rev. Lett.* **1996**, *77*, 3983.
(29) Spence, D.; Schultz, G. J. *J. Chem. Phys.* **1974**, *60*, 216.
(30) Dyne, P. J.; Jenkinson, W. M. *Can. J. Chem.* **1960**, *38*, 539.
(31) Dyne, P. J.; Jenkinson, W. M. *Can. J. Chem.* **1961**, *39*, 2163.
(32) Dyne, P. J.; Denhartog, J. *Can. J. Chem.* **1962**, *40*, 1616.
(33) Picard, J.-F. M.Sc. Thesis, Université de Sherbrooke, 1999.
(34) Doré, J.-F. M.Sc. Thesis, Université de Sherbrooke, 2003.
(35) Feulner, P.; Niedermayer, T.; Eberle, K.; Schneider, R.; Menzel, D.; Baumer, A.; Schmich, E.; Shaporenko, A.; Tai, Y.; Zharnikov, M. *Phys, Rev. Lett.* **2004**, *93*, 178302.
(36) DeRose, J. A.; Thundat, T.; Nagahara, L. A.; Lindsay, S. M., *Surf. Sci.* **1991**, *256*, 102.
(37) Paradis, E.; Rowntree, P. *J. Electroanal. Chem.* **2003**, *175*, 550.
(38) Kang, J.; Rowntree, P. *Langmuir* **1996**, *12*, 2813.
(39) Garand, E.; Picard J.-F.; Rowntree, P. *J. Phys. Chem. B* **2004**, *108*, 8182.
(40) Badia, A.; Cuccia, L.; Demers, L.; Morin, F.; Lennox, B. R. *J. Am. Chem. Soc.* **1997**, *119*, 2682.
(41) Buckingham, A. D.; Hentschel, H. G. E. *J. Polym. Phys. Ed.* **1980**, *18*, 853.
(42) Stanford Research Systems, private communication.
(43) Rapp, D.; Sharp, T. E.; Brigatta, D. D. *Phys. Rev. Lett*. **1965**, *14*, 533.
(44) Khakoo, M. A.; Segura, J. *J. Phys. B* **1994**, *27*, 2355.
(45) The exact energy depends on the fate of the incident electron. Calculations are based on the gas-phase thermochemistry data from NIST Chemistry WebBook for methane, propane, hydrogen and the related radicals and anions, http://webbook.nist.gov.
(46) Melton, C. E. *J. Chem. Phys.* **1972**, *57*, 4218.
(47) Engquist, I.; Liedberg, B. *J. Phys. Chem.* **1996**, *100*, 20089.
(48) Pépin, C. M.Sc. Thesis, Université de Sherbrooke, 2001.
(49) Hauchard, C.; Pépin, C.; Rowntree. P. A. *J. Phys. Chem. B.* Submitted for publication.